Energy quay walls

Performance analysis and optimisation

Gerola, Marco; Cecinato, Francesco; Leclercq, Vincent; Vardon, Philip J.

DOI
10.1016/j.gete.2025.100664

Publication date
2025

Document Version
Final published version

Published in
Geomechanics for Energy and the Environment

Geomechanics for Energy and the Environment 42 (2025) 100664

Contents lists available at ScienceDirect

Geomechanics for Energy and the Environment

journal homepage: www.elsevier.com/locate/gete

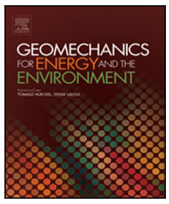

Energy quay walls: Performance analysis and optimisation

Marco Gerola [a,*], Francesco Cecinato [a], Vincent Leclercq [b], Philip J. Vardon [c]

[a] Dipartimento di Scienze della Terra 'A. Desio', Università degli studi di Milano, Via Luigi Mangiagalli, 34, Milano, 20133, Italy
[b] CRUX Engineering BV, Phoenixstraat 28c, Delft, 2611 AL, The Netherlands
[c] Geo-Engineering Section, Delft University of Technology, PO Box 5048, Delft, 2600 GA, The Netherlands

ARTICLE INFO

Editors-in-Chief:
Professor Lyesse Laloui and Professor Tomasz Hueckel

Keywords:
Energy quay wall
Energy geostructures
Numerical modelling
Finite element method
Sheet pile wall

ABSTRACT

Energy Quay Walls (EQWs) are innovative energy geostructures with the unique capability to exchange heat with both soil and open water. Although previous laboratory testing demonstrated a promising energy efficiency for this type of system, its novelty necessitated thorough research to advance comprehension of its thermal behaviour and optimise energy efficiency. This paper conducts an in-depth examination of EQWs, employing numerical models validated against real data from a full scale test in Delft, The Netherlands.

Two Finite Element numerical models were developed to (i) reconstruct the undisturbed (i.e. pre-geothermal activation) temperature profile within the soil and (ii) conduct a comprehensive (3D) analysis of heat exchange processes in an EQW application (i.e. during geothermal activation), calibrating relevant parameters with field test data, providing valuable insights into its energy efficiency. Following validation, the geothermal activation model was employed to assess the impact of the flow regime within the heat exchanger pipes and the velocity of the open water on the energy efficiency of the EQW system. Additionally, the contributions of soil, water, and air to the energy gain are investigated. The results indicate that the primary source of energy gain is from open water, and the dominance of this contribution is further increased by the presence of turbulent flow within the heat exchanger pipes. However, the soil can play a key role in short term energy delivery. Furthermore, this study emphasises the importance of the open water movement, revealing a 48% reduction in energy extraction for fully stationary water scenarios.

1. Introduction

In recent decades, the need to shift away from fossil fuel dependency has substantially increased the utilisation of shallow ground source heating and cooling installations, which facilitate low-temperature heating and cooling systems. Consequently, ground source heat pump (GSHP) systems, are anticipated to make a substantial contribution to renewable energy provision.[1,2] Closed-loop ground source heat pump schemes include a sequence of ground heat exchangers forming a primary circuit and a building heating system constituting the secondary circuit. Key capital costs of these systems are the heat pumps and the construction of ground heat exchangers—where pipes must be installed into the ground. To mitigate this cost and reduce embodied energy, one approach is the utilisation of energy geostructures (EGs), where heat exchangers are embedded in structures providing both energy and structural support.[3]

Numerous studies have been dedicated to modelling the thermal and thermo-mechanical responses of EGs during both monotonic and cyclic extraction/injection of heat from/into the ground. These investigations encompass the most prevalent types of EGs, including Energy Piles (e.g., Refs. 4–11), Energy Tunnels (e.g., Refs. 12–16) and Energy Diaphragm Walls (e.g., Refs. 17–20), or the less widespread Energy Slabs,[3,21] Energy Barrettes,[3,22] Energy Anchors,[23] Energy Sewers,[24] Geothermal Pavements,[25] and Thermo-active Seal Panels.[26] The successful operation of numerous real-case installations of EGs[27] has motivated researchers and companies to explore and implement novel types of EGs through experimental testing and modelling. These include Energy Micro-piles[28–30] and Climate Roads.[31]

Recently, Energy Sheet Pile Walls have been proposed, where heat exchangers are attached to sheet piles used as retaining structures. Sheet piles are frequently used as retaining structures along waterways to create quay walls, and Energy Sheet Pile Walls can then be used in this application to exchange heat with both soil and open water. In this case they are also known as Energy Quay Walls (EQWs). Exploiting the significantly higher thermal conductivity of steel compared to concrete, sheet pile walls are well-suited for thermal activation.[32] An additional advantage of EQWs compared to other EGs is their possible use for the energy retrofitting of existing buildings, since the two structures are typically adjacent but not directly connected.

* Corresponding author.
E-mail address: marco.gerola@unimi.it (M. Gerola).

https://doi.org/10.1016/j.gete.2025.100664
Received 30 April 2024; Received in revised form 11 March 2025; Accepted 12 March 2025
Available online 21 March 2025

Ziegler et al.[33] conducted the first research on the energy behaviour of EQWs, utilising both large-scale laboratory tests and numerical modelling. The study examined two distinct thermal exchange systems: the first system employed conventional sheet pile configurations integrating heat exchanger pipes, while the second system featured prefabricated add-on elements featuring heat exchanger pipes mounted on a steel support plate and immersed in water. Their findings highlighted the significance of flow in the open water in determining system performance. The energy yield of the heat exchanger loops within the sheet pile sections ranged from 285 W/m (length here refers to a U-tube length) in the absence of flow in the open water to 430 W/m with its presence, whereas for the add-on elements, the efficiency varied from 550 W/m to 1750 W/m. This is compared to typically <50 W/m for heat exchanger piles in GSHP systems.[34] The high energy yield, even without open water flow, is thanks to natural convective phenomena occurring within the water body due to thermally-induced density gradients, which continually regenerated water temperatures. However, the limited implementation of EQW systems, despite its promising energy performance,[35] underscores the need for further research to comprehensively understand its thermal behaviour.

To gain deeper insights into the thermal behaviour of an actual EQW installation, a full scale EQW test site was developed located in Delft, The Netherlands, with the setup, operation and monitoring described by Vardon et al.[36] The field site EQW comprised three distinct heat exchanger piping systems: two involved deep and shallow steel heat exchanger U-pipes, with depths of 15 m and 3 m respectively, welded onto the sheet pile profile on the soil side, while the third system entailed add-on panels equipped with steel heat exchanger pipes, also with a depth of 3 m, mounted onto the sheet pile profile on the open water side. Vardon et al.'s findings underscore the critical influence of water temperature on the energy efficiency of all three systems, highlighting that the temperature within the soil at shallow depths is primarily influenced by variations in water and air temperatures rather than the heat exchange process itself. However, further investigation via numerical modelling allows deeper insights to be obtained into the energy behaviour of the system.

The energy performance of planar energy geostructures such as EQWs is expected to be influenced by multiple factors. These include the undisturbed ground temperature profile, thermal conductivity and specific heat of the soil, as well as various operational and construction parameters.[37,38] Regarding the undisturbed ground temperature, the initial geothermal energy available for extraction depends on the soil temperature profile, which is influenced by air temperature variations, especially near the surface. In the case of EQW installations, the presence and temperature of open water further modify the subsurface temperature profile. The available literature offers limited information on the undisturbed temperature profile within the soil surrounding a quay sheet pile wall. Analytical methods, mainly semi-empirical, have been developed to estimate the temperature distribution in the soil at various depths.[3,39] However, these methods typically assume a homogeneous soil half-space, neglecting the presence of different soil layers and the presence of open water at one of the domain boundaries. Consequently, these established methods may not adequately address the complexities associated with the actual subsoil conditions encountered in the EQW system.

In this study, to enhance the comprehension of the EQW thermal performance, two Finite Element (FE) numerical models were constructed utilising data obtained from the full scale test.[36] The primary objective of the first FE model, referred to as the 'Thermal Initialisation' model, was to reconstruct the temperature profile within the domain of interest prior to the geothermal activation of the EQW. The second FE model, termed the 'Geothermal Activation' model, aims to enable a comprehensive and accurate three-dimensional analysis of the heat exchange processes occurring within the EQW. Both FE models are validated using data collected from the full-scale test. Subsequently, the validated Geothermal Activation model is employed to assess the relative influence of crucial parameters, such as the flow regime within the heat exchanger pipes and velocity of the open water, on the energy performance of the EQW system.

2. Field test

A full-scale long-term experiment of an EQW was conducted in Delft, Netherlands, from October 2020 to July 2022 (Fig. 1(a)). The primary objective of this field trial was to gain a better understanding of the thermal energy extraction performance exhibited by the investigated system. Additionally, the full-scale test aimed to examine the influence of temperature cycles on the geotechnical behaviour.[40]

2.1. Layout

The EQW full-scale test comprises a quay wall, installed with sheet piles to a depth of 15 m and a length of 8 m, interfacing with a canal of 1.75 m in depth. The soil composition within the initial 20 m was determined through two distinct Cone Penetration Test (CPT) analyses. The composition consists of a 2 m thick layer of sand overlaying primarily clay, with sporadic occurrences of organic material or sand. The water table is close to ground level, resulting in the saturation of all identified soil layers. The installed EQW system integrated three distinct methods of including heat exchangers. In each case, heat exchangers comprising rectangular cross-section steel U-loop with external dimensions of 2 cm × 4 cm and a wall thickness of 3 mm. The first heat exchanger type, referred to as the 'shallow loop', had a depth of 3 m, and were specifically designed to exchange heat predominantly with the canal water. The lowermost 0.7 m of the heat exchanger were embedded into the soil with the uppermost 0.55 m in contact with air on one side and with soil on the other side. The second type, referred as the 'deep loop', extended to a depth of 15 m, that included 0.55 m in contact with air, 1.75 m in contact with open water and 12.7 m with soil, that were designed to extract thermal energy from both the soil and open water. The third type, known as 'add-on panels' had a depth of 3 m and shared the same contact length with water, soil and air of the shallow panels. Notably, while both the shallow and deep loops are welded directly on the sheet pile profile on the soil side and are installed during the sheet pile installation, the add-on panels can serve as energy retrofitting solutions for pre-existing quay walls.

The heat exchangers are connected in circuits of 3 U-tubes of the same type in series, with all circuits connected in parallel. The circuits attached to the sheet piles, i.e. the first two types described above, are illustrated in Fig. 1(b): purple and green correspond to the deep loops and red and blue denote the shallow loops. There are two circuits of each of the deep and shallow loops, and a single circuit of the add-on panels, leading to a cumulative total of 15 heat exchangers connected in 5 circuits within the EQW system. All U-loops were interconnected and linked to the heat pump through connection pipes made by high density polyethylene (HDPE), featuring a circular cross-section with a diameter of 32 mm. The heat exchanger liquid utilised was a water-glycol (80%–20%) mixture, chosen to prevent freezing even when operating at temperatures below 0 °C.

2.2. Instrumentation

An extensive monitoring system was deployed as depicted in Fig. 2. In total, 8 vertical thermistor strings were installed, incorporating 56 thermistor sensors in total. These strings were positioned at key positions around the EQW installation (green × symbols in Fig. 2). The thermistor strings were installed by pushing a steel tube into the soil, placing the thermistor string and filling with water.

On the deep loop activation side of the EQW (left side of Fig. 2), four thermistor sensor strings were installed. Among them, 'D_C' and 'D_B' were positioned at a distance of 1.5 m from the EQW system, in the canal and soil, respectively. These strings were equipped with a thermistor sensors at 2 m depth intervals. Additionally, the sensor strings 'D_FL' and 'D_FR' were located at distances of 0.42 m and 0.5 m from the EQW system, respectively. These strings were equipped with a thermistor sensors at 1 m depth intervals. Similarly, on the shallow

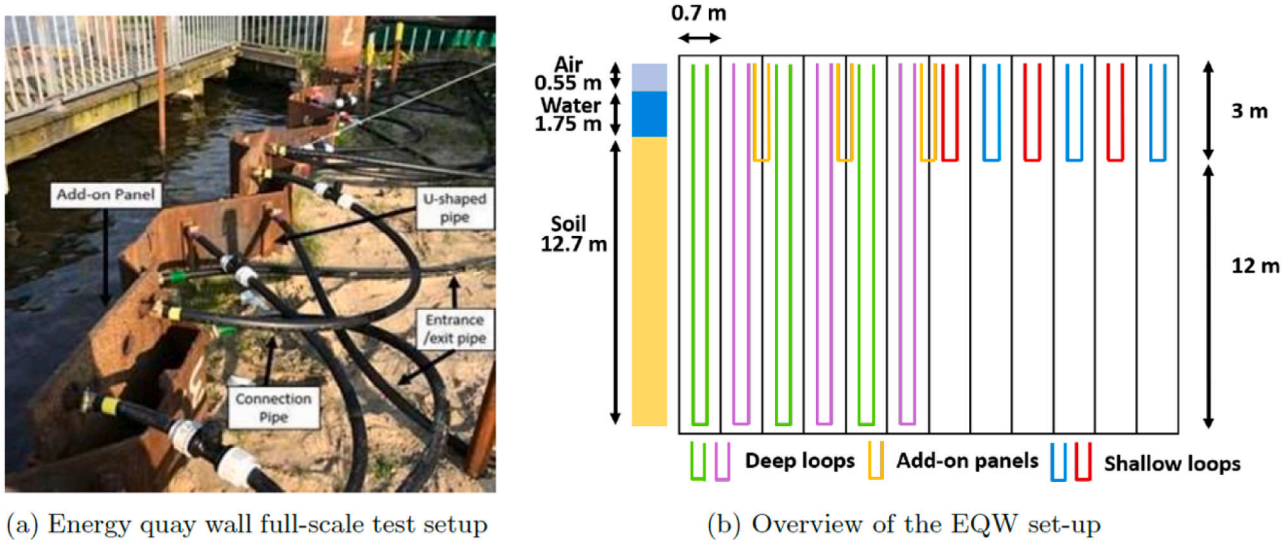

Fig. 1. Energy quay wall full-scale test installed in Delft (NL).

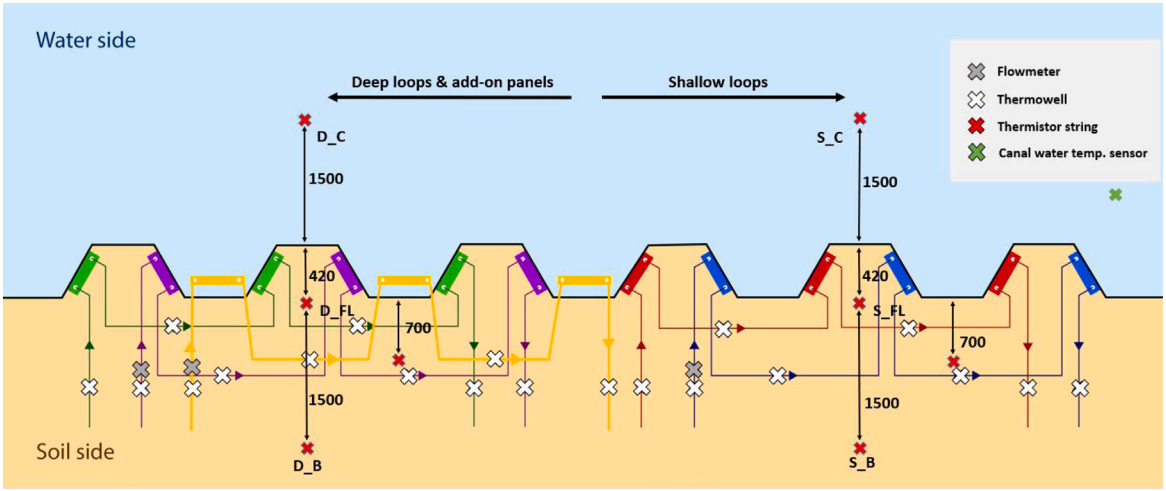

Fig. 2. Monitoring system setup.

loops side, four sensor strings, namely 'S_C', 'S_B', 'S_FL' and 'S_FR', were installed at the same distances from the EQW system. S_C was positioned in the canal, while S_B, S_FL and S_FR were placed in the soil (Fig. 2). The precise depth and location of the thermistors was detected by employing an inclinometer.

In addition, 20 thermowells, sensors inserted into the connection pipes with PT100-type temperature sensors, were positioned within the connection pipes at both the inlet and outlet points of each circuit, as well as between the series connections between every U-loop (red × symbols in Fig. 2). Additionally, two thermowells were installed at the inlet and outlet of the heat pump system. A total of five flow meters were installed at specific locations within the system: at the start of one of the deep loop circuits, one of the shallow loop circuits, the add-on panel circuit and at the outlet of the heat pump. An open water flow meter was placed in the canal to monitor the flow rate of the open water.

2.3. Operational phases

To comprehensively assess the thermal performance of all the circuits that define the EQW full-scale test, various operational phases were implemented. During each phase, specific combinations of shallow, deep and add-on panels were activated. This approach allowed for the independent analysis of the thermal performance of each circuit. The phases shown in Table 1 are:

- Comparative performance analysis and impact on soil temperature: the primary objective aimed to assess the performance of each circuit, comparing it to the performance achieved when all the deep or shallow circuits were in operation. The secondary objective involved investigating the impact of thermal activation on the soil temperature field. The inlet temperature of the heat exchanger loops was maintained within a range of −2 °C to 0 °C.
- Active regeneration assessment: fluid was circulated through the deep loops with the heat pump deactivated to investigate the system's ability to extract thermal energy from the open water and store it underground through passive circulation only. The inlet temperature of the heat exchanger loops was influenced by the temperature of the water and soil, varying approximately between 15 °C and 20 °C.
- Real heating demand: a replication of the heating load of realistic heating demand conditions was applied by activating the heat

Table 1
EQW full scale test operational phases.

Phase name	Activated circuit	Start day [day]	End day [day]	length [days]
Comparative performance 1	1 deep loop + 1 shallow loop	0	17	17
Comparative performance 2	2 deep loops	17	53	36
Comparative performance 3	2 shallow loops + add-on panel	53	123	70
Comparative performance 4	2 shallow loops	123	140	17
Comparative performance 5	2 deep loops	140	187	27
System off	None	187	216	27
Active regeneration 1	2 deep loops	216	310	96
System off	None	310	350	40
Active regeneration 2	2 deep loops	350	371	21
System off	None	371	385	14
Comparative performance 6	2 deep loops	385	415	30
Real heating demand	2 deep loops	415	491	76
Comparative performance 7	1 shallow loop + add-on panel	491	501	10
System off	None	501	506	5
Comparative performance 8	1 deep loop	506	526	20
Comparative performance 9	2 deep loop	526	593	67

pump for a cumulative period of 10–14 h per day. This approach emulated the intermittent heating demands commonly encountered in real-world applications. The inlet temperature of the heat exchanger loops was maintained within a range of −2 °C to 0 °C.

3. Numerical model

3.1. Governing equations

Conservation of energy is used as the governing equation to allow simulation of the thermal energy. In the EQW-water-soil system, the principal mechanisms governing the heat exchange are conduction and convection. Heat transfer within the soil is assumed to be primarily governed by conduction, with convection effects considered negligible. This assumption simplifies the model and is supported by two factors: (i) the absence of significant seepage flow between the canal and the ground at the validation site, and (ii) findings by Ziegler et al.,[33] who demonstrated that groundwater flow has minimal impact on the energy performance of EQW systems. Convection is the dominant mechanism of heat transfer within the heat carrier fluid in the heat exchanger pipes, between the heat carrier fluid and the steel pipe walls, with conduction and convection governing the heat exchange mechanisms within the open water, air above the water and between the open water and the soil.

In reality, additional thermal phenomena may occur, such as thermal radiation at the soil surface and convective heat transfer in the pore water due to groundwater flow. Radiant heat exchange is generally considered negligible except in the coarsest of soils[41,42] and the likelihood of groundwater convection at the field test site is low thanks to the prevalence of low-permeability soils, mostly clay, within the initial 15 m of depth, and the mainly static phreatic level.

The conservation of energy equation can then be written as the transient heat diffusion equation (e.g., Ref. 43):

$$\rho C_p \frac{\partial T}{\partial t} + \rho C_p(\mathbf{u}\cdot\nabla T) - \nabla\cdot\lambda\nabla T = Q_{wall} \tag{1}$$

where ρ is the density of the material [kg/m^3], C$_p$ is the fluid specific heat capacity [J/kgK], T is the temperature [K], t is time [s], $\mathbf{u}$ is the fluid velocity [m/s], λ is the thermal conductivity of the medium [W/mK] and Q$_{wall}$ is the heat or sink source employed to couple the heat extraction from the heat exchanger pipes.

To simulate the thermal energy transfer within the pipes, a one-dimensional formulation has been adopted to allow for a simplified representation of the heat transfer processes:

$$A_p\rho_f C_{pf}\frac{\partial T}{\partial t} + A_p\rho_f C_{pf}(\mathbf{u_p}\cdot\nabla T) - \nabla\cdot A_p\lambda_f\nabla T - f_D\frac{\rho_f A_p}{2d_h}\left|\mathbf{u_p}^3\right| = q'_{wall} \tag{2}$$

where $\mathbf{u}_p$ is the cross-section average fluid velocity field along the tangent of the centre line of the pipes [m/s], A_p is the pipe cross-section area available for flow [m^2], ρ_f is the fluid density [kg/m^3], C_{pf} is the fluid specific heat capacity at constant pressure [J/kgK]. The term $q'_{wall} = -Q_{wall}A_p$ represents the radial heat exchange through the pipe walls and is calculated as $Q_{wall} = hZ(T_{ext} - T)$, where h is the effective heat flow coefficient, Z is the pipe perimeter and T_{ext} is the external temperature.

In Eq. (2), the last term on the left-hand side represents the heat dissipated by internal friction within the fluid, i.e. the energy loss due to viscous effects and fluid motion within the pipes. The Darcy friction factor, f_D, characterises the head drop occurring along the heat exchanger pipes and is expressed as a function of the Reynolds number (Re) and the ratio of surface roughness (e) to hydraulic diameter (d_h). It is determined using the Churchill equation, which applies to all flow regimes, namely laminar flow (occurring when $Re < 2100$ (e.g., Ref. 44)), transient flow ($2100 < Re < 4000$) and turbulent flow ($Re \geq 4000$):

$$f_D = 8\left[\left(\frac{8}{Re}\right)^{12} + \left(\left[-2.457\ln\left(\left(\frac{7}{Re}\right)^{0.9} + 0.27\left(\frac{e}{d_h}\right)\right)\right]^{16} + \left(\frac{37530}{Re}\right)^{16}\right)^{-1.5}\right]^{1/12} \tag{3}$$

3.2. Numerical investigation

Two FE numerical models were formulated utilising the COMSOL Multiphysics software, building up on preliminary model versions.[45,46] The first model, termed the 'Thermal initialisation' model, was developed to assess the initial temperature distribution preceding the thermal activation of the EQW system. The second model, referred to as the 'Geothermal activation' model, was employed to execute an extensive investigation into the thermal behaviour and performance of the EQW system. Further details on the numerical settings can be found in Ref. 47

3.2.1. Thermal initialisation

The model domain has a parallelepipedal shape with dimensions of 26 m in width, 33 m in length, and 20 m in height, as shown in Fig. 3, while the width and depth of the EQW located at the domain centre, are 8.4 m and 15.0 m respectively.

The model domain is divided into different soil layers as outlined in Table 2, each characterised by its unique thermal properties. In addition to the soil layers, two additional layers were incorporated: one for the open water of the canal and one to simulate the presence of air above the open water. The latter is essential in the context of the geothermal activation model (see Section 3.2.2) to prevent any segment

Table 2
Layers characterisation.

Material type	Layer thickness m	(Bulk) Density kg/m^3	Thermal conductivity W/mK	Specific heat capacity J/kgK
Sand	2	2000	1.8	1200
Clay with Peat	3.7	1600	0.6	2000
Silty clay	1	1900	1.2	1200
Sandy clay	1.5	1900	1.6	1200
Silty clay	1.5	1900	1.2	1200
Clay	10.3	1900	1.4	1200
Water	1.75	1000	0.6	4186
Air	0.55	1	0.024	1000

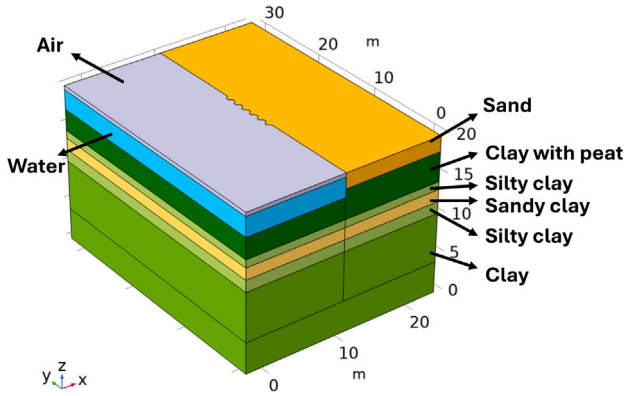

Fig. 3. Configuration of the numerical model domain and subdivision into distinct soil layers.

of the heat exchanger pipes from extending beyond the boundaries of the model domain. Elements which will eventually represent the sheet piles are included in this model, but allocated properties of the soil in the layer which they are in, as such allowing the easy later inclusion of the sheet piles, but having no impact on this model. The determination of soil density, heat capacity, and thermal conductivity was based on empirical correlations derived from the results of a cone penetrometer test conducted near the EQW.[48] These estimations were further corroborated by cross-referencing existing geological data from data set.[49] These bulk thermal properties were assigned to the solid domain elements, while the properties of water and air were taken from the literature (e.g., Ref. 50). A total of 85572 tetrahedral elements were uniformly generated to ensure an appropriate level of detail for accurate analysis.

A horizontal velocity value of 0.001 m/s was assigned to the open water layer to represent the measured velocity of the canal water. Additionally, a wind velocity of 0.05 m/s was specified to the air layer to replicate a scenario characterised by low wind speed (e.g. Ref. 51).

The lateral and base domain boundaries were positioned at a considerable distance from the EQW, allowing an accurate analysis of the heat transfer processes specifically associated with the EQW itself, without being influenced by the lateral boundary conditions. The bottom boundary of the model domain was assigned a fixed temperature of 12 °C, representing the undisturbed subsurface temperature at this location. This value is in accordance with readings acquired from the most deeply located thermistors described in Section 2.2, but also in accordance with undisturbed temperature conditions observed at neighbouring locations.[52] Thermal insulation was applied to the lateral boundaries to prevent heat transfer through those surfaces. The canal flow was considered by employing inflow and outflow boundary conditions, at the locations indicated on Fig. 4(b). A similar approach was adopted for the airflow within the air domain (applied as shown on Fig. 5(b)).

To account for the seasonal variations in air and water temperatures, a yearly sinusoidal interpolation was applied based on the measured temperature data at a weather station located 4 km from the site from the previous two or three years. These sinusoidal curves, representing the temperature variation throughout the year, were repeated ten times to cover a simulation period of ten years (Figs. 5(a) and 4(a)). The interpolated air temperature was assigned to all the top boundary surfaces (Fig. 5(b)), while the interpolated water temperature was assigned as the inflow temperature for the open water domain (Fig. 4(b)).

The initial temperature within the soil was set everywhere equal to the average undisturbed temperature (12 °C). To compare the numerical results with the data collected from the monitoring system, the temperature at a total of 56 points within the domain was monitored, corresponding to the positions of the installed thermistors.

The simulation conducted for thermal initialisation spanned a period of 10 years and was executed with a timestep of 1 day. It was found through numerical experimentation that using smaller mesh elements and a smaller timestep yielded similar results. Thus, these settings were selected to balance computational efficiency and accuracy.

3.2.2. Geothermal activation

In the Geothermal activation numerical model, several changes are introduced compared to the Thermal initialisation model. Specifically, the heat exchanger loops that characterise the EQW case study, as depicted in Fig. 6, are incorporated into the model. These heat exchanger loops consist of vertically oriented steel U-loops with an inner cross-sectional dimension of 0.014 m × 0.034 m and a surface roughness of 0.046 mm. Additionally, the steel loops are connected by horizontally oriented HDPE pipes, which have an inner diameter of 28 mm and a surface roughness of 0.0015 mm. These HDPE pipes link the steel U-loops both to the secondary circuit (not simulated, but represented by the inlet temperature boundary condition) and to each other. Moreover, the simulation does not model the thickness of the quay wall, as it is significantly smaller than the overall extension of the model domain.

The Geothermal activation numerical model was modified from the Thermal initialisation model by adjusting properties and boundary conditions to accurately represent the EQW system and simulate its thermal behaviour: (i) The thermal conductivity of 45 W/mK was assigned to the steel heat exchanger pipes, while a value of 0.4 W/mK was assigned to the HDPE material constituting the connection pipes. (ii) The heat exchanger fluid was simulated as a mixture of 80% water and 20% glycol, which reduces the freezing point of the water. The thermal conductivity, specific heat capacity, dynamic viscosity, and density of the water-glycol mixture were prescribed as constants of 0.48 W/mK, 3691 J/(kgK), 1040 kg/m^3 and 0.002314 Pa s, respectively.[53] (iii) The boundary conditions for the model encompassed the locally detected air temperature assigned to the top surface, water temperature assigned to the inflow section, and the fluid temperature at the inlet of each loop. Furthermore, the detected fluid velocity in each loop was incorporated as a time-dependent function. Details regarding this input data are presented in the Appendix. (iv) In addition to the points measuring the temperature in the model domain corresponding to each thermistor, five additional probe points were introduced in the FE model to detect the simulated temperature of the heat exchanger fluid at the outlet of each loop corresponding the position of the thermowells installed

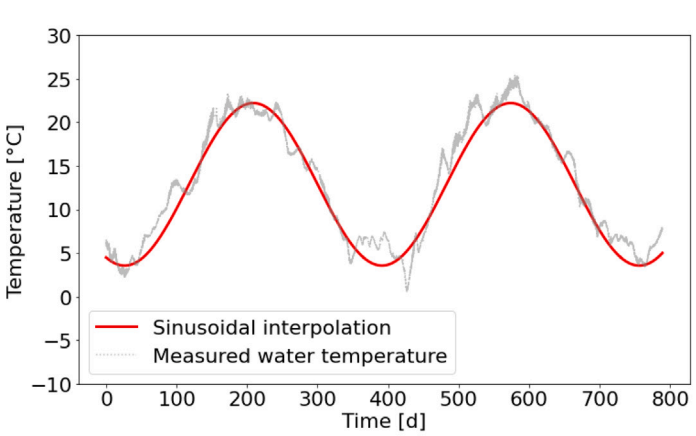

(a) Sinusoidal temperature boundary value and measured data

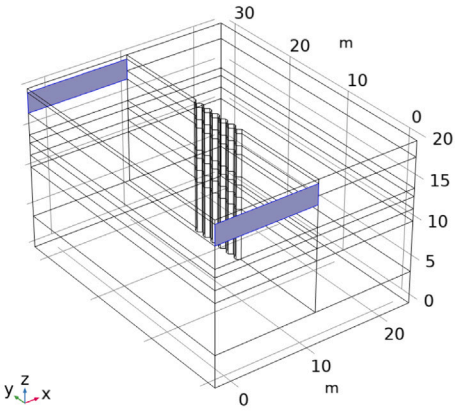

(b) Boundaries where the inflow and outflow conditions are imposed

Fig. 4. Water boundary conditions.

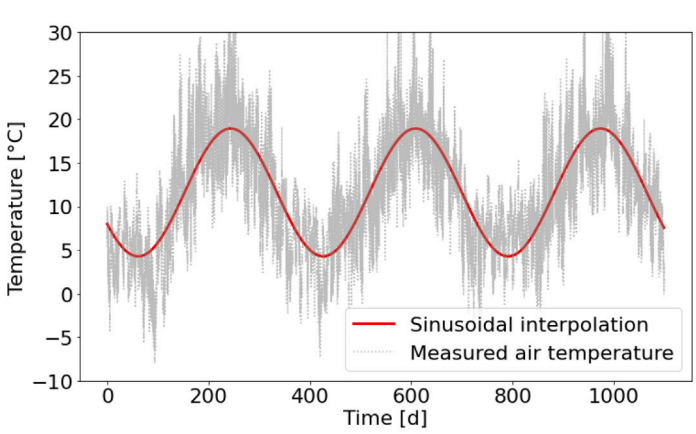

(a) Sinusoidal temperature boundary value and measured data

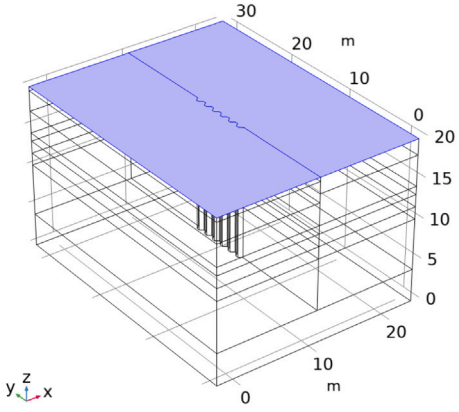

(b) Boundaries where the conditions are imposed

Fig. 5. Air boundary conditions.

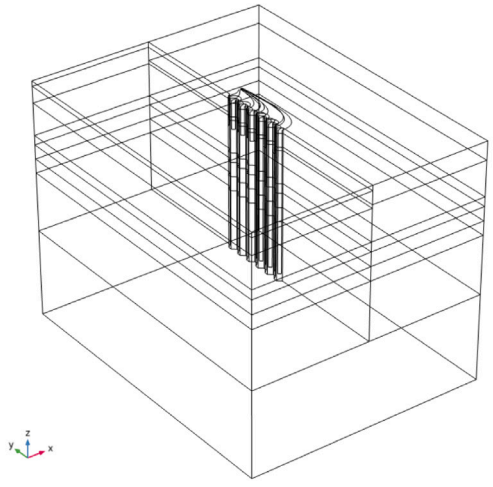

(a) Computational domain

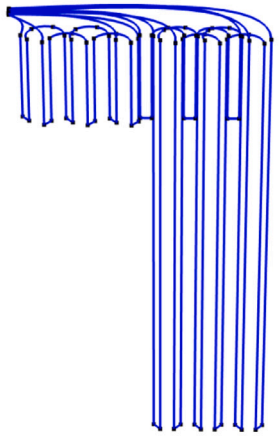

(b) Representation of heat exchanger pipes using 1D line simplification

Fig. 6. Geothermal activation model geometry.

in the monitoring system in the full scale test. (v) The temperature distribution resulting from the thermal initialisation model was set as the initial temperature distribution for the whole domain. (vi) A new tetrahedral mesh with a total of 233697 tetrahedral elements was generated in order to refine the mesh in the model domain surrounding the EQW and have it coarser near the lateral model boundaries to enhance calculation accuracy near the heat exchanger whilst keeping computational time reasonably low. (vii) The EQW thermal operation simulation was divided into two periods: one with the heat pump active 24 h a day, and the other one with the heat pump active between 10 and 16 h a day. Two different maximum timestep values were adopted for each period, to optimise simulation accuracy: 1 day for the first period and 0.1 day for the second one. (viii) The temperature data collected from the monitoring system were taken every 15 min, which is much lower than the timestep used in the simulation. To ensure representative data, averages were taken based on the numerical timestep value to evaluate all the time-dependent input data.

4. Numerical model validation

4.1. Thermal initialisation

To assess the accuracy of the initial soil temperature profile for the geothermal activation model, a comparison was conducted between the numerical simulation results and the recorded temperature values at monitoring points corresponding to the two thermistor strings 'D_FL' and 'D_FR' which feature the highest number of sensors. This comparison was carried out using the average root mean square error (RMSE) (Fig. 7) between the simulated and measured data (prior to geothermal activation). The RMSE was calculated after each year of simulation.

The RMSE values decrease dramatically after the first year of simulation for both sensor strings. There is virtually no difference in the numerical model results after 6 years, leading to consistent RMSE values thereafter; these values closely match those obtained in the first year, indicating accurate reproduction of the soil temperature profile after a single year of simulation. In Fig. 8, the depth profiles of temperature obtained from the 'D_FR' and 'D_FL' sensor strings are plotted alongside the corresponding numerical model results after 10 years of simulation. This figure visually confirms the consistency between the simulated and measured temperature profiles, thereby demonstrating the efficacy of the numerical model. Fig. 9 illustrates the temperature distribution within the soil domain following the 10-year simulation period. It is observed that due to the impact of the water and air temperature boundary conditions, there are significant vertical thermal gradients over the first 5 m depth. Additionally, the presence of the water body only on one side of the domain leads to a notable horizontal thermal gradient. This indicates the necessity of numerical modelling to accurately simulate the initial thermal conditions of the model before the EQW geothermal activation.

4.2. Geothermal activation

The geothermal activation of the EQW system was simulated for the entire 2-year test duration in one simulation, encompassing various operational phases. The initial 27 day period of geothermal activation were excluded, during which a comprehensive system integrity check was conducted and the collected data were thought to not be reliable.

In Fig. 10, a comparison is presented between the measured temperature difference between the inlet and outlet of the heat pump and the corresponding simulated temperature difference. In Fig. 10(a), the Comparative performance analysis is shown, with Fig. 10(b) presenting the Real heating demand phase. The times presented begin after the 27 day start-up period.

Fig. 11 presents the soil temperature variations at depths of 10 m, 11 m and 12 m, with Fig. 11(a) presenting the Comparative performance analysis and Fig. 11(c) presenting the Real heating demand phase.

Concerning the temperature differences observed during the Comparative performance phase (the initial 187 days depicted in Fig. 10(a)), the numerical model reproduces well the temperature differences
throughout, indicating that it can simulate the complex heat exchange processes occurring under a range of different operating conditions. Nonetheless, a few discrepancies between numerical results and real data emerge during three specific periods. In the first period, spanning from day 17 to day 49, only one deep loop circuit was active. During the first three days the flow rate demonstrated a declining trend, reducing by one third. The high variation in flow rate on a daily basis could introduce errors if the daily average data is utilised as input parameters for the simulations. Additionally, throughout this period, there were difficulties in accurately collecting temperature data at the outlet of the heat pump, which was set as 0 °C based on the limited measurements available. During the second period, from day 50 to day 62, both shallow loops and add-on panels were active. The hydraulic system experienced insufficient pressurisation and only a minor flow rate was detected in the deep loops, which are considered inactive. These technical issues are not replicated in the model, and they may contribute to discrepancies between the numerical results and the measured data. In the third period, from day 123 to day 140, both the add-on panels and one shallow circuit were operational. However, due to the absence of data on the flow rate within the shallow circuit, simulations were conducted assuming only the add-on panels active. In the third period, from day 123 to day 140, both the shallow circuits were operational. No specific issues were reported during this period. Notably, the numerical temperature difference mirrored the fluctuations in water temperature over time, which initially decreased and then began to increase from day 134. In contrast, the measured temperature difference continued to decline throughout the entire period resulting in anomalous behaviour.

Regarding the temperature variation within the soil shown in Fig. 11(a), a closely comparable trend is observed in both numerical simulations and test data. Notably, when the deep loops are active, a decrease in soil temperature is noted, while their inactivity leads to an increase in soil temperature through natural passive conduction. A slight discrepancy with a maximum of approximately half a degree between numerical results and measured temperatures is evident during both temperature increase and decrease. This discrepancy may be associated with the precise positioning of thermistor sensors within the soil; even slight alterations in their positions could lead to changes in the magnitude of temperature variation. In terms of the real heating demand phase, both the temperature difference between the inlet and outlet of the heat pump and the temperature variation within the soil, as shown in Figs. 10(b) and 11(c), are well simulated by the model, with relatively minor variations in both cases. These results highlight the capability of the numerical model to capture the complex heat exchange processes occurring within the EQW system during its thermal activation phases.

An illustration of the temperature distribution in the model domain at the conclusion of the Comparative performance phase, i.e., at the end of heat extraction on day 187, and of the active regeneration phase, i.e. day 310, is presented in Fig. 12. The cold plume is clearly observed surrounding the deep loops after heat extraction is complete (Fig. 12(a)), and the significantly higher temperature at the surface and in the open water is observed (indicating a much higher thermal gradient between the water and the heat exchanger pipes). After active thermal regeneration (Fig. 12(b)), a higher temperature zone immediately adjacent to the deep loops is seen. This temperature is higher than the ambient temperature at that depth, indicating the recharge has restored and initial temperature and stored addition energy. Note

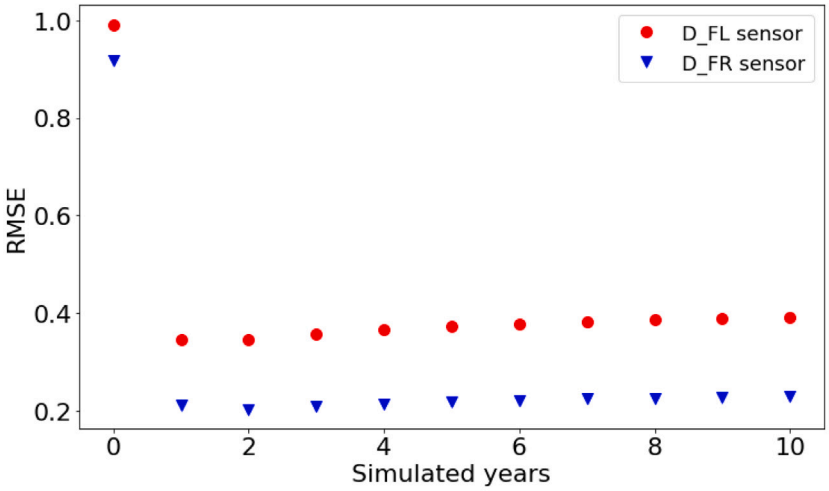

Fig. 7. Root Mean Square Error (RMSE) for each of the 10 years of thermal initialisation simulation compared to both the D_FL and D_FR sensor strings field data.

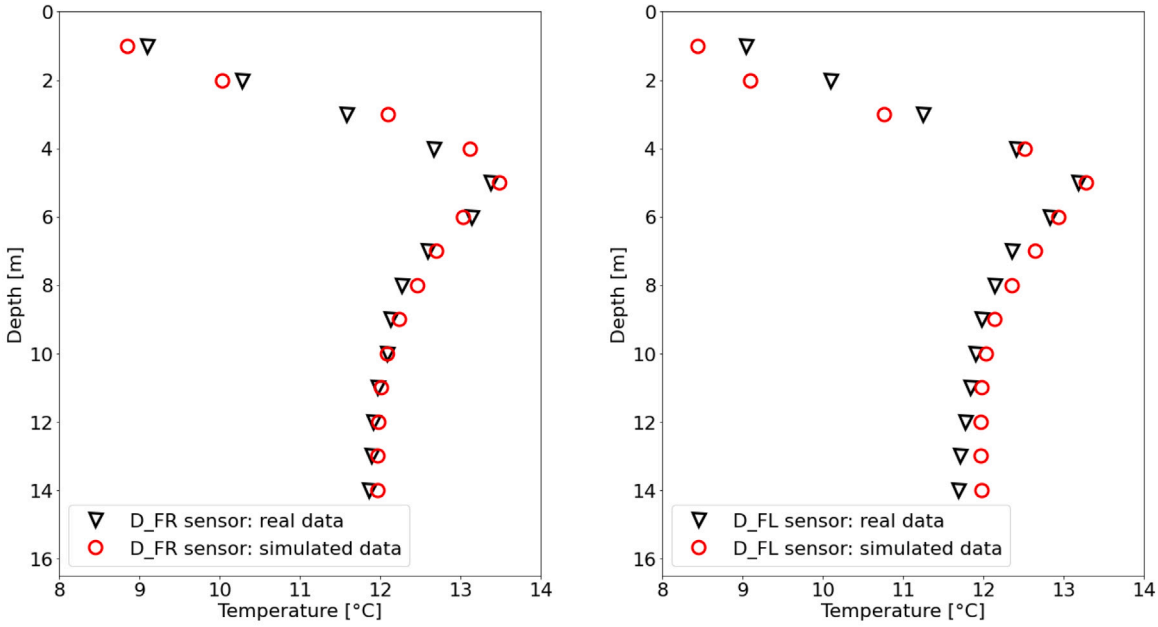

(a) D_FL sensor (b) D_FR sensor

Fig. 8. Temperature into the soil before the geothermal activation of the quay wall.

that this active recharge does not use a heat pump, so the energy input to achieve this is negligible. At this time, it is also seen that the water body is colder that the soil immediately below and adjacent to it, due to the colder external air temperature.

5. Exploratory investigation of the EQW performance

An exploratory investigation was conducted to examine the primary factors influencing the enhancement of energetic performance of the EQW system. The impact of the circulating fluid velocity, an analysis of whether the thermal energy is extracted from soil, water or air is undertaken and a comparison of a stationary and moving water body are undertaken. The energy performance can be assessed using the exchanged energy through time. The heat exchange power q can be determined using the formula:

$$q(t) = \dot{m} C_p [T_{in}(t) - T_{out}(t)] \quad (4)$$

where T_{in} and T_{out} are the inlet and outlet temperatures of the heat pump $[K]$, respectively, and $\dot{m}$ denotes the mass flow rate of the fluid [kg/s]. The inlet temperature and the mass flow rate are input values measured by the monitoring system while the outlet temperature is derived from the validated geothermal activation numerical model presented in Section 4.2.

Two distinct phases were identified for the study to allow an analysis of the roles played by the shallow loops with the add-on panels and the deep loops, respectively: the first phase, denoted as ‘Phase 1’, encompassed the activation of the shallow loops and add-on panels from day 75, following the initial geothermal activation of the EQW system, until day 140. The subsequent phase, labelled as ‘Phase 2,’ spanned from day 141 to day 187 and focused solely on the operation of the deep loops.

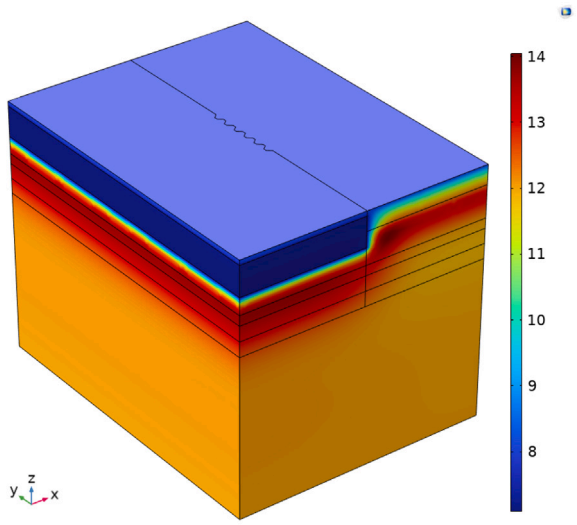

Fig. 9. Temperature distribution across the domain following a 10-year thermal initialisation period.

5.1. Effect of turbulent flow regime

As depicted in Fig. 13(a) the Reynolds number achieved in the circulating fluid in the field tests is shown. In both Phase 1 and 2, it was equal to or less than 2100, representing a laminar flow regime. An alternative simulation was carried out, where the flow velocity of the heat exchanger fluid was doubled to achieve a Reynolds number equal to or greater than 4000 (Fig. 13(b)), i.e., turbulent flow.

In Fig. 14(a), the total thermal power obtained during both Phase 1 and Phase 2 is illustrated, showing an increase by 51% and 62%, respectively, when switching from laminar to turbulent flow. This emphasises the significance of achieving turbulent fluid flow within the EQW system to enhance its energy efficiency. This outcome is achieved by doubling the flow rate velocity within the heat exchanger pipes indicating that the temperature difference between the inlet and outlet of the heat pump is reduced 14(b), though not by half.

The influence of fluid flow rate within the heat exchanger pipes on energy output has been highlighted by previous studies on energy piles and energy tunnels. You et al.[54] and Gao et al.[55] conducted experiments on energy pile sites, investigating three distinct flow rates: low, medium, and high. A 49% increase was observed in the heat rejection rate for a double U-tube when the flow transitioned from low to medium. Similarly, You et al. obtained comparable results for a cement-fly ash-gravel pile, showing a 38% increase in heat exchange rate per meter length of the pile when transitioning from low to medium flow rates. Minor differences were observed in both cases when further increasing the flow velocity from medium to high, although no information on flow regime and Reynolds number was provided.

Concerning energy tunnels, Buhmann et al.[56] conducted tests at the Stuttgart–Fasanenho test plant, manipulating the flow rate within the heat exchanger pipes. They found that increasing the Reynolds number from 2400 to 4330 resulted in a roughly 50% increase in the extraction rate.

The slightly higher increment observed for the EQW system, particularly for the deep loops in Phase 2, is likely attributed to the flow of open water, which naturally regenerates the open water temperature. Additionally, the higher thermal conductivity and lower thickness of steel compared to the concrete layer, (present in both energy piles and energy tunnels), contributes to energy exchange enhancement. This results in a lower thermal resistance in the EQW system compared to both energy piles and energy tunnels.

5.2. Energetic impact of increasing flow rate

Achieving turbulent flow improves the energy extraction rate of the EQW system. On the other hand, increasing the fluid flow velocity brings about larger energy expenditure at the system's circulation pump. In this section, an analysis is carried out comparing the required increment in hydraulic energy against the net energy gained through turbulent flow.

The hydraulic power P_h, representing the power necessary for the motion of the water-glycol mixture through the heat exchanger pipes, can be calculated as follows[57]:

$$P_h = \dot{m} g H_L \tag{5}$$

where g is the gravitational constant, and H_L denotes the total head loss within the system [m]. The overall head loss H_L in the piping system encompasses the head loss attributable to viscous effects in the straight pipes, designated as the major loss H_{Lmajor}, and the head loss incurred in diverse pipe components, referred to as the minor loss H_{Lminor}:

$$H_L = H_{Lmajor} + H_{Lminor} \tag{6}$$

The major loss is assessed for both the steel and HDPE heat exchanger pipes as follows:

$$H_{Lmajor} = f_D \frac{L}{d_h} \frac{\rho_f u^2}{2} \tag{7}$$

where L is the length of the heat exchanger pipes [m]. The comparative analysis is conducted for both Phase 1 and Phase 2. During the initial days of Phase 1, spanning from day 53 to day 123 (hereafter termed Phase 1a), both the shallow loops and add-on panels are activated. In this phase, the length of the steel heat exchanger pipes amounts to 54 m, Subsequently, from day 123 to 136 (hereafter termed Phase 1b), only the shallow loops are operational, and length is 36 m. The length of the connecting HDPE pipes is approximated to be 53 m and 31 m in the respective phases. In Phase 2, the overall length of the steel pipe extends to 180 m, accompanied by an estimated total HDPE connection pipe length of 48 m.

Concerning the minor loss, the assessment of alterations in the cross-sectional shape, along with the bends in the U-loop, is carried out as follows[57]:

$$H_{Lminor} = K_L \frac{u^2}{2g} \tag{8}$$

where K_L represents the loss coefficient, taking values of 0.06 and 0.05 for the contraction and expansion of the cross-sectional area of the pipes, respectively. Both phenomena manifest three occurrences within the circuit. The loss coefficient attributed to bends is established at 0.2. It is noteworthy that the head loss induced by monitoring sensors installed in the pipes is deemed negligible and consequently omitted from this consideration.

Table 3 presents the net energy gained and the hydraulic energy introduced into the system to double the flow velocity, achieving turbulent flow within the heat exchanger pipes for both Phase 1 and Phase 2. It can be observed that for both phases, the net hydraulic energy value constitutes less than 1% of the corresponding net energy gained. Consequently, the net hydraulic energy is nearly negligible in comparison to the net energy gained. This underscores that achieving turbulent flow in the EQW system is a key strategy for enhancing the energy performance.

5.3. Energy gained from soil, water and air layers

The energy gained from different parts of the domain is significant to understand the system performance. The U-tubes were split into pipe segments (i) in contact with soil on both sides, (ii) in contact with open

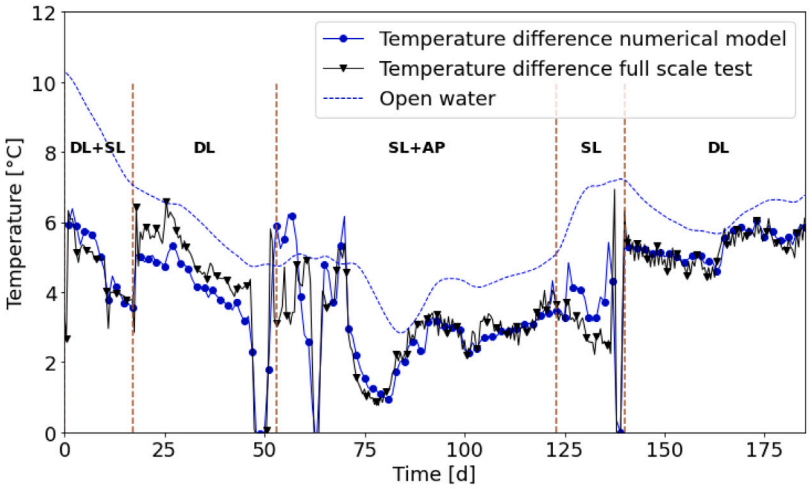

(a) Comparative performance analysis

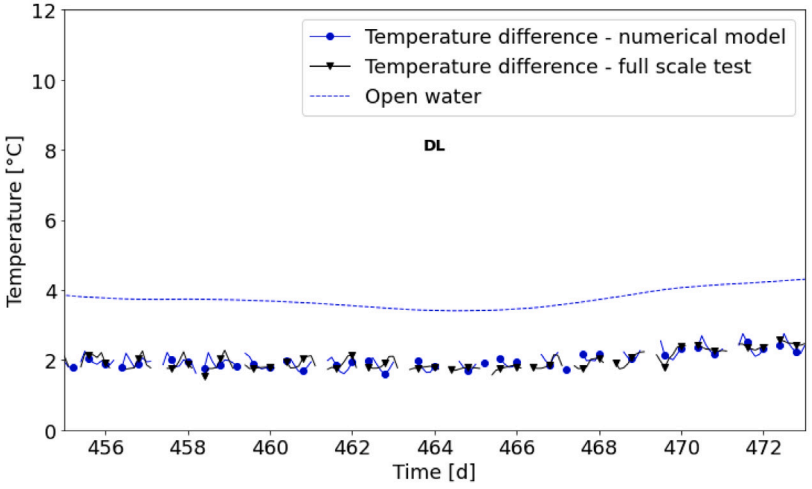

(b) Real heating demand phase

Fig. 10. Temperature difference between the inlet and outlet of the heat pump. The figures depict the periods when the heat pump was active. SL = shallow loops, DL = deep loops, AP = add-on panels.

Table 3
Hydraulic energy expenditure and the net energy gained in the transition from laminar to turbulent flow.

	Net hydraulic energy [kJ]	Net energy gained [kJ]
Phase 1	0.29	134.84
Phase 2	0.46	61.26

water on one side and soil on the other side, (iii) in contact with air on one side an with soil on the other side.

The contributions of soil, water, and air to the total energy gained were calculated for one of the shallow loop circuits, comprising three U-loops connected in series, as depicted in Fig. 15(a) during Phase 1, when both shallow loops and add-on panels were active. The energy extracted from the open water predominantly influences the overall energy gain. The 0.5 m length embedded in the soil appears to have a negligible impact on energy performance, while the 0.55 m length featuring air and soil on opposite sides exerts a more substantial influence.

As shown in Fig. 16, during the first 7 days, the air temperature remains predominantly below 0 °C, with the water temperature being approximately 2 °C higher. In this period around 90% of the thermal energy is extracted from the water, with just over 5% from the air and just under 5% from the soil.

After the initial 7 days, the rise in air temperature leads to an increment in the percentage of energy gained from the air layer, reaching a maximum of almost 20%, while the energy percentages gained from both the water and soil layers slightly decrease before stabilising at a constant value, despite further increases in air temperature, with its maximum value in Phase 1 on day 125.

Between day 110 and day 122, there is a notable increase of approximately 4% in the proportion energy gained from the water layer. During this specific time frame, only one of the shallow loop circuits, in conjunction with the add-on panels, was operational, while the other one was closed. This condition reduces the overall thermal extraction from the water (as one shallow loop is closed), resulting in an increment in the proportion of the energy gained from the water layer as the water layer close to the EQW is cooled down less. This situation is distinct from the remaining days of Phase 1, where both shallow loop systems are simultaneously active. This indicates also a limited influence in the performance of the EQW when increasing density of the heat exchanger pipes in a water body. The transition from laminar to turbulent flow in shallow loops seems to have a limited impact on the percentages of acquired energy.

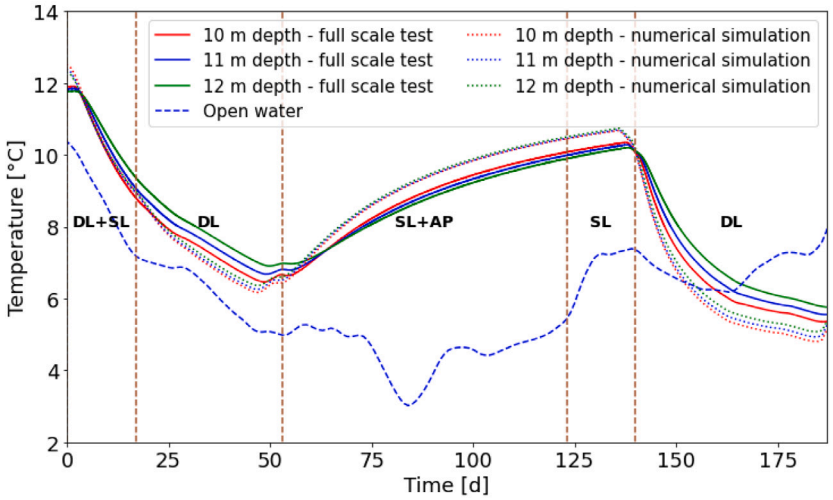

(a) Comparative performance analysis

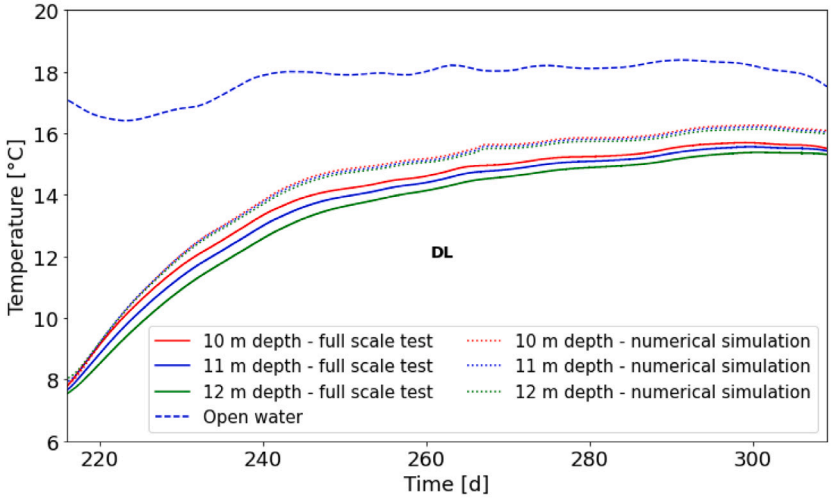

(b) Passive and active regeneration assessment

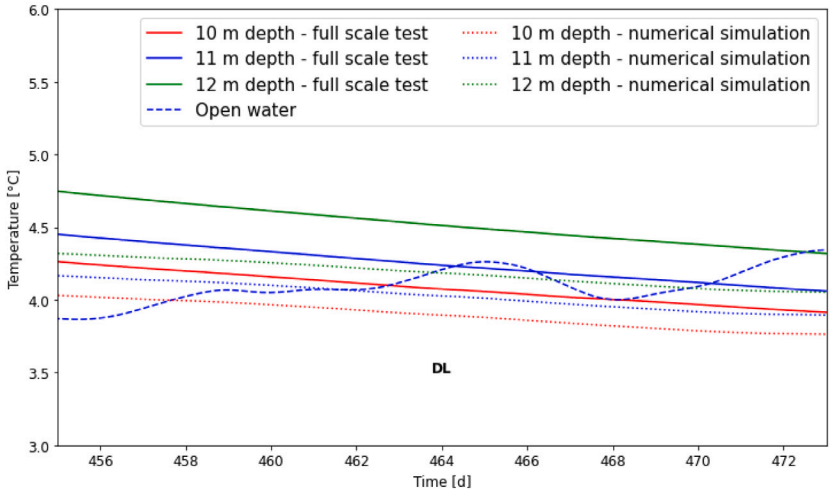

(c) Real heating demand phase

Fig. 11. Temperature variation in the soil. SL = shallow loops, DL = deep loops, AP = add-on panels.

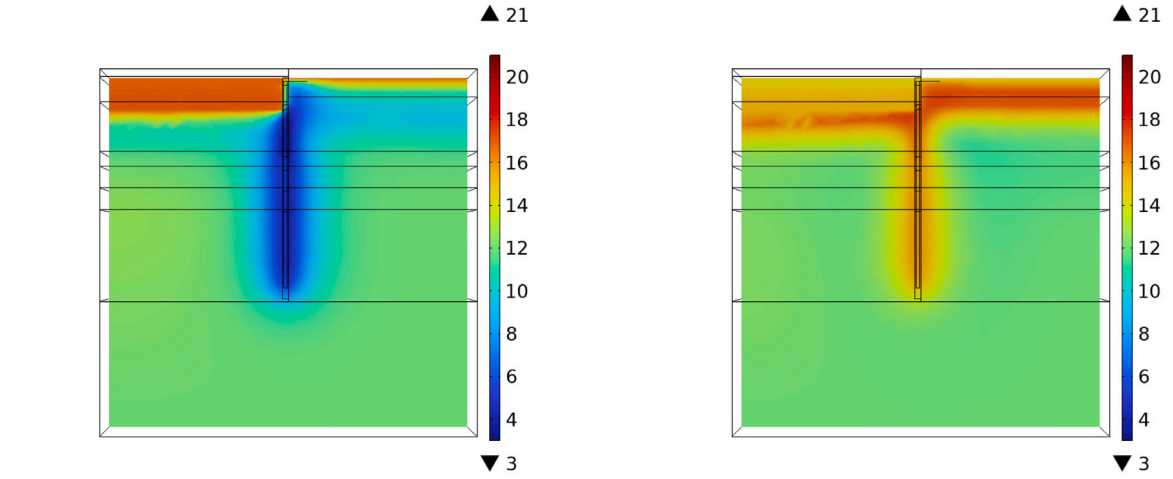

(a) After 187 days of the comparative performance analysis. (b) After active regeneration at 310 days.

Fig. 12. Temperature distribution within the soil domain.

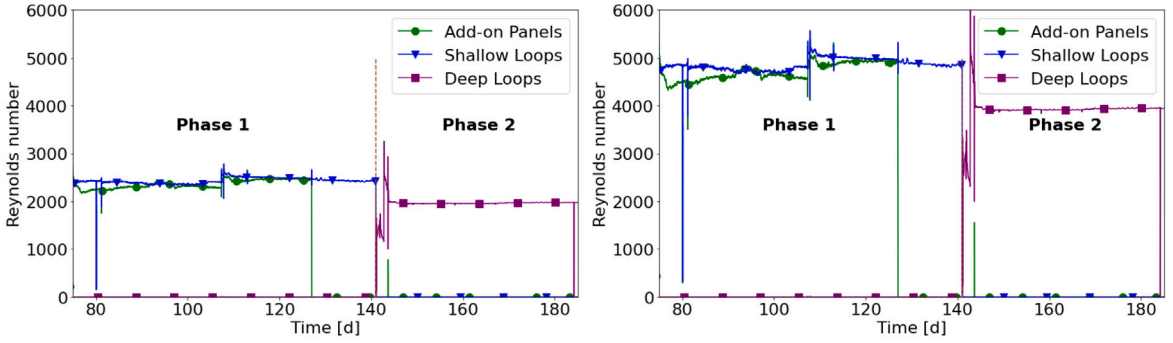

(a) Values from experimental data of Phase 1 and 2 (b) Values obtained by increasing the flow velocity

Fig. 13. Calculated Reynolds number values for different flow conditions in Phase 1 and 2.

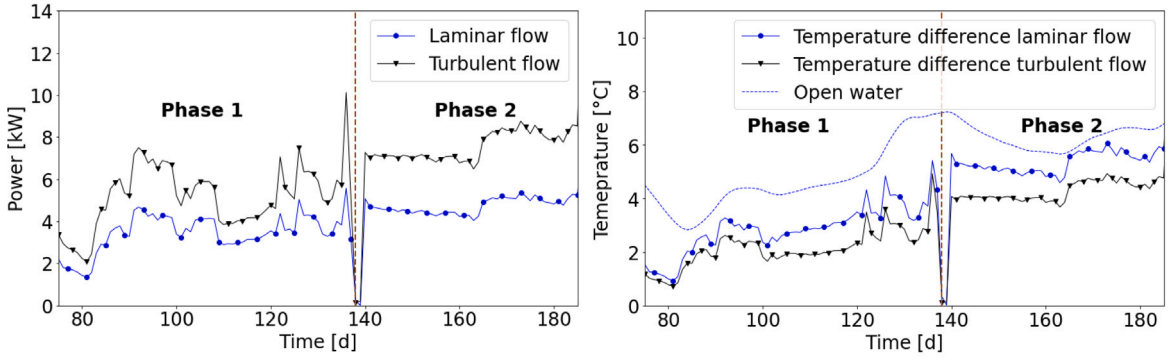

(a) Power extraction (b) Temperature difference

Fig. 14. Power extraction and temperature difference between the inlet and outlet of the heat pump comparison: laminar flow versus stationary turbulent flow.

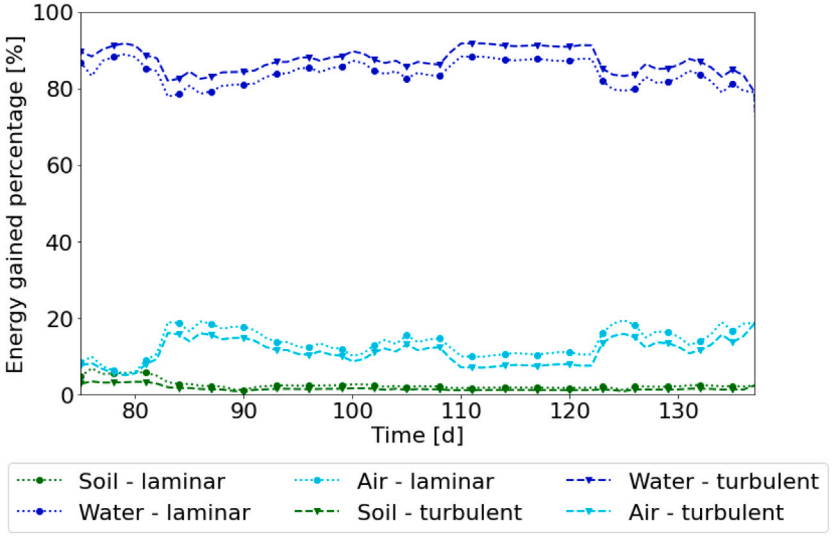

(a) Phase 1

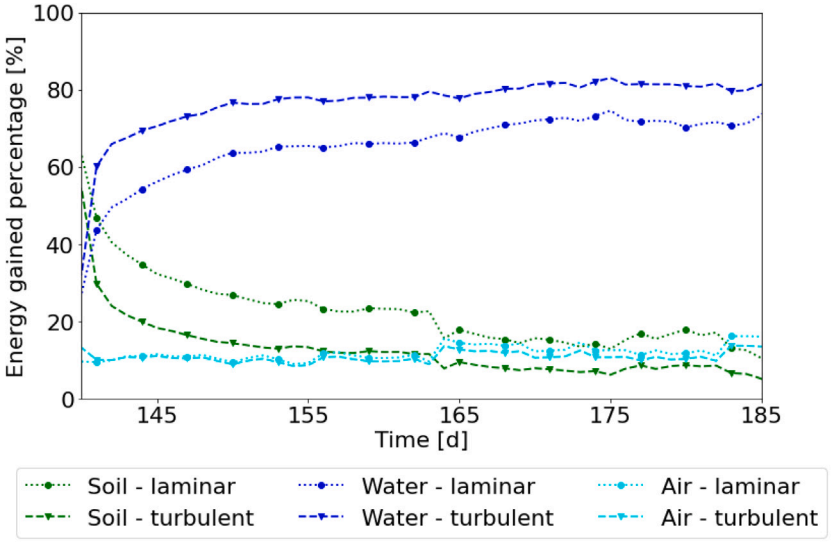

(b) Phase 2

Fig. 15. Comparative energy extraction.

The comparison is similarly conducted for one of the active deep loop circuits during Phase 2, as depicted in Fig. 15(b). On the first day (day 139), 50% of the total energy is derived from the soil layer, while 41% is obtained from the water layer, and 9% from the air layer. Over the subsequent 8 days, the energy gained from the soil decreases from 50% to a more constant value of 24%. The diminishing power extracted from the soil over time aligns with the early stages of thermal activation observed in energy piles (or other EGs fully embedded in soil), where efficiency declines initially before stabilising around a constant value. This phenomenon is attributed to the rapid decrease in soil temperature during the initial stages (e.g. Ref. 3). It is noteworthy that both the air and water temperatures, after day 163, exhibit a rapid increase of 7 °C as illustrated in Fig. 16. Consequently, the contribution from the soil layer decreases by a maximum of 5%. This behaviour indicates the buffering behaviour of the soil, allowing higher extraction when it is cold for limited time periods. The additional costs for installing longer heat exchanger pipes and operating longer systems, need to be balanced against higher performance in more extreme weather periods.

Transitioning from laminar to turbulent flow leads to an increase in the energy acquired from the water in the deep loops. In this scenario, starting from three days after the initiation of thermal activation in the deep loops, less than 20% of the power is gained from the soil layer, despite the significantly longer embedded length in the soil.

5.4. Effect of stationary open water condition

As previously demonstrated,[33] open water assumes a paramount role in energy extraction. The dynamics of open water are hypothesised as a crucial determinant for replenishing water temperature in the proximity of the EQW system and enhancing the overall system efficiency.

Fig. 17(a) depicts the comparison between the power obtained from the validated numerical model and the power that would be acquired by assuming stationary open water, thus disregarding potential phenomena that could influence water movement, such as natural

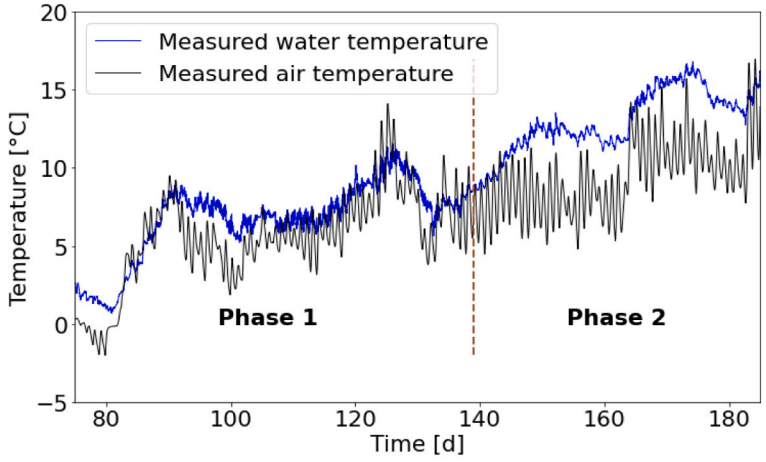

Fig. 16. Detected air and water temperatures throughout the duration of phase 1 and phase 2.

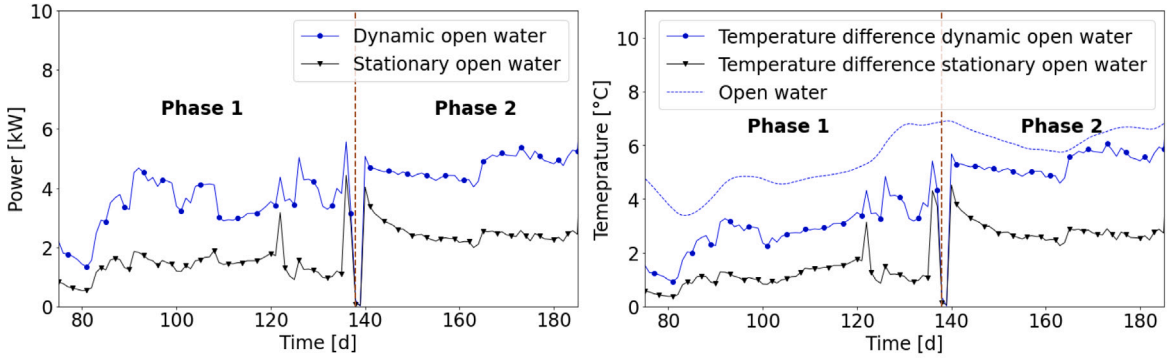

(a) Power extraction (b) Temperature difference

Fig. 17. Power extraction and temperature difference between the inlet and outlet of the heat pump comparison: dynamic open water versus stationary open water.

convection and wind currents. The water temperature variations are contingent solely upon external temperature fluctuations.

The total energy gained in both Phase 1 and Phase 2 exhibits a reduction of 48% in case of stationary open water. This highlights the pivotal role of open water flow in influencing the energy performance of the EQW system. It should be noted, as demonstrated in Ziegler et al.,[33] that even a minimal open water flow significantly enhances the energy efficiency of the system. That study indicates that the specific value of the open water flow has minimal impact on the energy output. In many real situations, it is likely that a minor (local) water flow will occur, due to many processes such as wind, boat movement and natural thermal gradients, as well as bulk water flow. This reduction in power is reflected by the reduction in the temperature difference between the inlet and the outlet of the heat pump (Fig. 17(b)).

6. Conclusions

Two numerical models were built and employed to investigate the performance of an Energy Quay Wall (EQW) system, i.e., the 'Thermal initialisation' model, designed to investigate the temperature profile within the soil prior to the thermal activation of the EQW system, and the 'Geothermal activation' model, dedicated to analysing the energy performance of the system. The models were validated using real data and the 'Geothermal activation' model was subsequently utilised to investigate key factors influencing the energy performance of the EQW system. Key conclusions are as follows:

- In cases where water and air temperature data are available, thermal initialisation proves to be a suitable method for determining an accurate initial temperature profile within the soil before the geothermal activation of the EQW system.
- The majority of the energy is obtained from the water system, even when significantly more heat exchanger pipes are embedded in the soil.
- The soil provides a transiently decreasing energy output, whereas the water can provide a more stable output in time. However, the energy extracted from the water is impacted more strongly by the external air temperature, whereas the soil provides a time limited buffer.

- The transition to a turbulent flow regime within the heat exchange pipes significantly enhances the energy efficiency of the system. A shift from laminar to turbulent flow by doubling the flow rate resulted in a 51% and 62% increase in energy extraction for shallow loops — add-on panels and deep loops, respectively. The additional energy required to achieve turbulent flow is negligible.
- Under turbulent flow conditions, the open water becomes more critical in the energy extraction process for deep loops, contributing around 80% of the total energy extracted from the deep loop. This value surpasses the 60% contribution observed under laminar flow. Conversely, for shallow loops, both laminar and turbulent flows yield 80% of the total energy extraction from the open water layer.
- The flow of open water is observed as a crucial parameter for the energy efficiency of the EQW system. In a scenario with stationary open water, a 48% reduction in the total energy extracted is observed for both shallow and deep loops.

EQWs can be generally regarded as a viable geothermal solution, akin to other Energy Geostructure types, as they eliminate the need for dedicated installations and can be installed close to existing buildings. They have been shown by both field experimentation and numerical analysis to provide significant amounts of renewable energy for space heating purposes.

CRediT authorship contribution statement

Marco Gerola: Writing – review & editing, Writing – original draft, Visualization, Software, Methodology, Formal analysis, Conceptualization. **Francesco Cecinato:** Writing – review & editing, Methodology, Conceptualization, Supervision, Funding acquisition. **Vincent Leclercq:** Writing – review & editing, Methodology, Conceptualization. **Philip J. Vardon:** Writing – review & editing, Methodology, Conceptualization, Supervision.

Declaration of Generative AI and AI-assisted technologies in the writing process

During the preparation of this work the author(s) used ChatGPT in order to improve language and readability. After using this tool/service, the author(s) reviewed and edited the content as needed and take(s) full responsibility for the content of the publication.

Declaration of competing interest

The authors declare that they have no known competing financial interests or personal relationships that could have appeared to influence the work reported in this paper.

Acknowledgements

Support under the Italian Ministry of University's "PON - DM 1061/2021" scheme, co-funded by CRUX Engineering BV, and the Kansen voor West S.P.O.E.D. KvW3-00036 program is gratefully acknowledged. M. Gerola and F. Cecinato also acknowledge the support received by GEOREFIT - Closing knowledge gaps on energy geostructures for retrofitting of buildings and infrastructures", funded by European Union – Next Generation EU, Mission 4, Component 1, CUP E53D23002670006, within the PRIN 2022 program (2023-2025, D.D.104-02/02/2022, Ministero dell'Università e della Ricerca, Italy).

Appendix. Additional model inputs

This appendix encompasses all time-dependent input data obtained from the monitoring system employed in the EQW full scale test. The data include the temperature at the inlet of the heat exchanger pipes (Fig. A.18), the flow rates within the shallow loops, deep loops, and add-on panels (Fig. A.19), and the recorded air and water temperatures (Fig. A.20).

Data availability

Data will be made available on request.

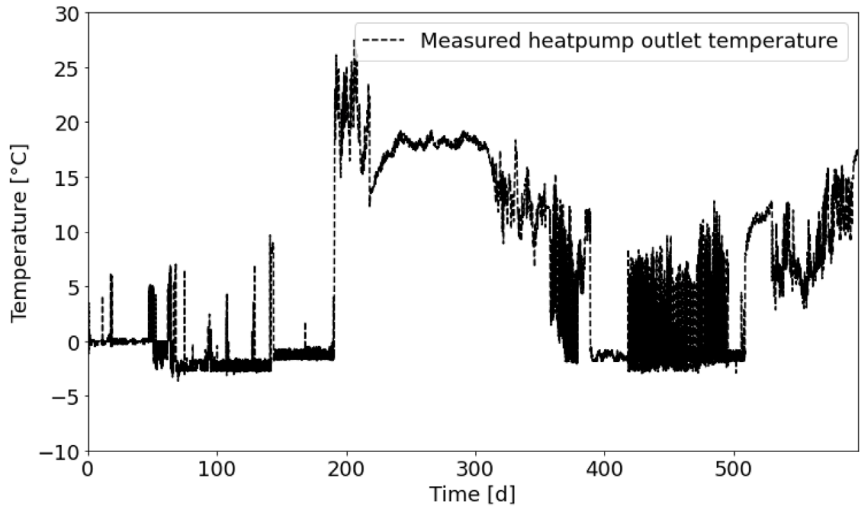

Fig. A.18. Measured temperature at the outlet of the heatpump over the entire duration of the full-scale testing.

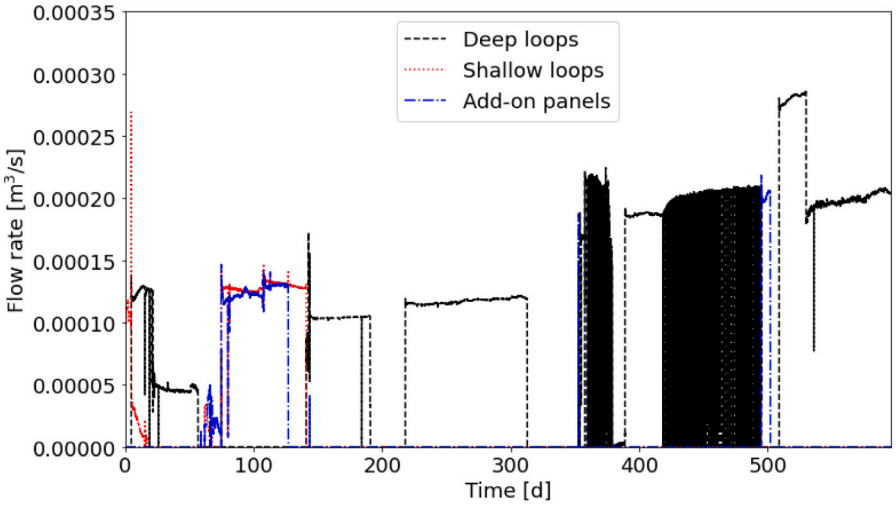

Fig. A.19. Measured flow rates within the deep loops, shallow loops and add-on panels over the entire duration of the full-scale testing.

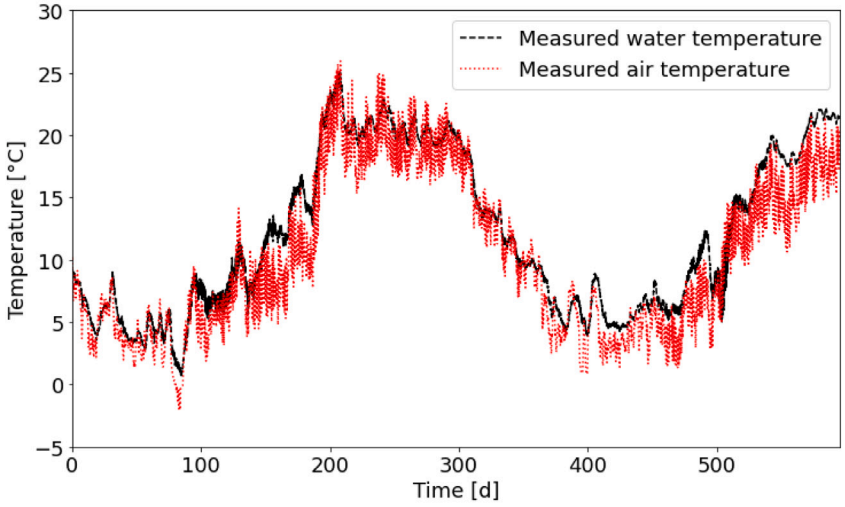

Fig. A.20. Measured air and water temperature over the entire duration of the full-scale testing.

References

1. Lund JW, Freeston DH, Boyd TL. Direct utilization of geothermal energy 2010 worldwide review. *Geothermics*. 2011;40(3):159–180. http://dx.doi.org/10.1016/j.geothermics.2011.07.004.
2. Sanner B. *Summary of EGC 2019 Country Update Reports on Geothermal Energy in Europe*. European Geothermal Congress 2019 Den Haag; 2019:11–14.
3. Brandl H. Energy foundations and other thermo-active ground structures. *Geotechnique*. 2006;56:81–122. http://dx.doi.org/10.1680/geot.2006.56.2.81.
4. Fadejev J, Simson R, Kurnitski J, Haghighat F. A review on energy piles design, sizing and modelling. *Energy*. 2017;122:390–407. http://dx.doi.org/10.1016/j.energy.2017.01.097.
5. Cecinato F, Loveridge FA. Influences on the thermal efficiency of energy piles. *Energy*. 2015;82:1021–1033. http://dx.doi.org/10.1016/j.energy.2015.02.001.
6. Loveridge F, Cecinato F. Thermal performance of thermoactive continuous flight auger piles. *Environ Geotech*. 2016;3:265–279. http://dx.doi.org/10.1680/jenge.15.00023.
7. Bourne-Webb PJ, Freitas TMB. Thermally-activated piles and pile groups under monotonic and cyclic thermal loading–A review. *Renew Energy*. 2020;147:2572–2581. http://dx.doi.org/10.1016/j.renene.2018.11.025.
8. Di Donna A, Laloui L. Numerical analysis of the geotechnical behaviour of energy piles. *Int J Numer Anal Methods Geomech*. 2015;39:861–888. http://dx.doi.org/10.1002/nag.2341.
9. Bourne-Webb PJ, Amatya B, Soga K. A framework for understanding energy pile behaviour. *Proc Inst Civ Eng: Geotech Eng*. 2013;166:170–177. http://dx.doi.org/10.1680/geng.10.00098.
10. Salciarini D, Ronchi F, Tamagnini C. Thermo-hydro-mechanical response of a large piled raft equipped with energy piles: a parametric study. *Acta Geotech*. 2017;12:703–728. http://dx.doi.org/10.1007/s11440-017-0551-3.
11. Batini N, Rotta Loria AF, Conti P, Testi D, Grassi W, Laloui L. Energy and geotechnical behaviour of energy piles for different design solutions. *Appl Therm Eng*. 2015;86:199–213. http://dx.doi.org/10.1016/j.applthermaleng.2015.04.050.
12. Ogunleye O, Singh RM, Cecinato F, Choi JC. Effect of intermittent operation on the thermal efficiency of energy tunnels under varying tunnel air temperature. *Renew Energy*. 2020;146:2646–2658. http://dx.doi.org/10.1016/j.renene.2019.08.088.
13. Bidarmaghz A, Narsilio GA. Heat exchange mechanisms in energy tunnel systems. *Geomech Energy Environ*. 2018;16:83–95. http://dx.doi.org/10.1016/j.gete.2018.07.004.
14. Barla M, Di Donna A. Energy tunnels: concept and design aspects. *Undergr Space (China)*. 2018;3:268–276. http://dx.doi.org/10.1016/j.undsp.2018.03.003.
15. Insana A, Barla M. Experimental and numerical investigations on the energy performance of a thermo-active tunnel. *Renew Energy*. 2020;152:781–792. http://dx.doi.org/10.1016/j.renene.2020.01.086.
16. Ogunleye O, Singh RM, Cecinato F. Assessing the thermal efficiency of energy tunnels using numerical methods and Taguchi statistical approach. *Appl Therm Eng*. 2021;185:116377. http://dx.doi.org/10.1016/j.applthermaleng.2020.116377.
17. Bourne-Webb PJ, Freitas TMB, Gonçalves RADC. Thermal and mechanical aspects of the response of embedded retaining walls used as shallow geothermal heat exchangers. *Energy Build*. 2016;125:130–141. http://dx.doi.org/10.1016/j.enbuild.2016.04.075.
18. Di Donna A, Cecinato F, Loveridge F, Barla M. Energy performance of diaphragm walls used as heat exchangers. *Proc Inst Civ Eng: Geotech Eng*. 2017;170:232–245. http://dx.doi.org/10.1680/jgeen.16.00092.
19. Sterpi D, Coletto A, Mauri L. Investigation on the behaviour of a thermo-active diaphragm wall by thermo-mechanical analyses. *Geomech Energy Environ*. 2017;9:1–20. http://dx.doi.org/10.1016/j.gete.2016.10.001.
20. Makasis N, Narsilio GA, Bidarmaghz A, Johnston IW, Zhong Y. The importance of boundary conditions on the modelling of energy retaining walls. *Comput Geotech*. 2020;120:103399. http://dx.doi.org/10.1016/j.compgeo.2019.103399.
21. Sterpi D, Tomaselli G, Angelotti A. Energy performance of ground heat exchangers embedded in diaphragm walls: Field observations and optimization by numerical modelling. *Renew Energy*. 2020;147:2748–2760. http://dx.doi.org/10.1016/j.renene.2018.11.102.
22. Rotta Loria AF, Ravera E, Laloui L. Thermo-hydro-mechanical behavior of energy barrettes: Field experiments and numerical simulations. *Geomech Energy Environ*. 2023;34:100451. http://dx.doi.org/10.1016/j.gete.2023.100451.
23. Mimouni T, Dupray F, Laloui L. Estimating the geothermal potential of heat-exchanger anchors on a cut-and-cover tunnel. *Geothermics*. 2014;51:380–387. http://dx.doi.org/10.1016/j.geothermics.2014.02.007.
24. Adam D, Markiewicz R. Energy from earth-coupled structures, foundations, tunnels and sewers. *Geotechnique*. 2009;59:229–236. http://dx.doi.org/10.1680/geot.2009.59.3.229.
25. Makasis N, Gu X, Kreitmair MJ, Narsilio GA, Choudhary R. Geothermal pavements: A city-scale investigation on providing sustainable heating for the city of Cardiff, UK. *Renew Energy*. 2023;218:119248. http://dx.doi.org/10.1016/j.renene.2023.119248.
26. Kürten S. Use of geothermal energy with thermo-active seal panels. In: *Geotechnical Engineering: New Horizons. Proceedings of the 21st European Young Geotechnical Engineers' Conference*. Rotterdam, Netherland: IOS Press; 2011:327–332. http://dx.doi.org/10.3233/978-1-60750-808-3-327.
27. Di Donna A, Barla M, Amis T. Energy geostructures: Analysis from research and systems installed around the world. In: *DFI 2017: 42nd Annual Conference on Deep Foundations*. 2017:1–11.
28. Cecinato F, Salciarini D. Energy performance assessment of thermo-active micropiles via numerical modeling and statistical analysis. *Geomech Energy Environ*. 2022;29:100268. http://dx.doi.org/10.1016/j.gete.2021.100268.
29. Ronchi F, Salciarini D, Cavalagli N, Tamagnini C. Thermal response prediction of a prototype energy micro-pile. *Geomech Energy Environ*. 2018;16:64–82. http://dx.doi.org/10.1016/j.gete.2018.07.001.
30. Gerola M, Lupattelli A, Cecinato F, Salciarini D, Arola T. Numerical analysis of the behaviour of energy micropiles used for heat storage: A case study in Turku (Finland). Berlin/Heidelberg, Germany: Springer Science and Business Media Deutschland GmbH; 2023:808–815. http://dx.doi.org/10.1007/978-3-031-34761-0_97,
31. Poulsen SE, Andersen TR, Tordrup KW. Full-scale demonstration of combined ground source heating and sustainable urban drainage in roadbeds. *Energies*. 2022;15(12):4505. http://dx.doi.org/10.3390/en15124505.
32. Haasnoot J, Vardon PJ, Pantev I, Bersan S, Bloemers B, Smeulders D. Energy quay walls. 2020:06002. In: E3S Web of Conferences; vol. 205, http://dx.doi.org/10.1051/e3sconf/202020506002.
33. Ziegler M, Koppmann D, Pechnig R, Knapp D. Energy sheet pile walls–experimental and numerical investigation of innovative energy geostructures. In: *Conf. Proc. XVII European Conference on Soil Mechanics and Geotechnical Engineering, Reykj, Avik, Iceland*. 2019.
34. Loveridge F, McCartney JS, Narsilio GA, Sanchez M. Energy geostructures: A review of analysis approaches, in situ testing and model scale experiments. *Geomech Energy Environ*. 2020;22. http://dx.doi.org/10.1016/j.gete.2019.100173.
35. Koppmann D. *Untersuchung der thermischen Aktivierung von Stahlspundwänden* (Ph.D. thesis). RWTH Aachen University; 2021.
36. Vardon PJ, Gerola M, Leclerq V, de Jong K, Haasnoot JK, Janssen R, Stoelhorst P, Pantev I, de Vries J, Bersan S, Smeulders D, Cecinato F. The energy quay wall: results from a full-scale field test. 2024 [Manuscript submitted].
37. Kürten S, Mottaghy D, Ziegler M. Design of plane energy geostructures based on laboratory tests and numerical modelling. *Energy Build*. 2015;107:434–444. http://dx.doi.org/10.1016/j.enbuild.2015.08.039.
38. Kürten S, Mottaghy D, Ziegler M. A new model for the description of the heat transfer for plane thermo-active geotechnical systems based on thermal resistances. *Acta Geotech*. 2015;10:219–229. http://dx.doi.org/10.1007/s11440-014-0311-6.
39. Hillel D. *Introduction to Environmental Soil Physics*. San Diego, Calif.: Academic Press; 1982.
40. De Vries J. *Quays Rather Than Boilers Extracting Heat From Water and Soil Through Energy Sheet Piles* (Master's thesis). Delft University of Technology; 2021.
41. Rees SW, Adjali MH, Zhou Z, Davies M, Thomas HR. Thermal response prediction of a prototype energy micro-pile. *Renew Sustain Energy Rev*. 2000;4:213–265. http://dx.doi.org/10.1016/S1364-0321(99)00018-0.
42. Fillion M-H, Côté J, Konrad J-M. Thermal radiation and conduction properties of materials ranging from sand to rock-fill. *Can Geotech J*. 2011;48(4):532–542. http://dx.doi.org/10.1139/t10-093.
43. Lewis RW, Schrefler BA. *The Finite Element Method in the Static and Dynamic Deformation and Consolidation of Porous Media*. Chichester, UK: Wiley; 1998.
44. Munson BR, Young DF, Okiishi TH, Huebsch W. *Fundamentals of Fluid Mechanics*. Hoboken, NJ: Wiley; 2009.
45. Gerola M, Cecinato F, Haasnoot JK, Vardon PJ. Analisi numerica del comportamento termico di UNA palancola energetica. In: *Incontro Annuale dei Ricercatori Geotecnica (IARG 2022) Proceedings*. Caserta, Italy: 2022.
46. Gerola M, Cecinato F, Haasnoot JK, Vardon PJ. Numerical modelling of energy quay walls to assess their thermal behaviour. In: *Symposium of Energy Geotechnics Proceedings*. Delft, Netherland: 2023.
47. Gerola M, Cecinato F, Haasnoot JK, Vardon PJ. Understanding the thermal efficiency of energy quay walls: A comprehensive study using field tests and finite element simulations. In: *COMSOL Conference Proceedings*. Munich, Germany: 2023.
48. Vardon PJ, Peuchen J. CPT correlations for thermal properties of soils. *Acta Geotech*. 2021;16:635–646. http://dx.doi.org/10.1007/s11440-020-01027-2.
49. Dalla Santa G, Galgaro A, Sassi R, Cultrera M, Scotton P, Mueller J, Bertermann D, Mendrinos D, Pasquali R, Perego R, Pera S, Di Sipio E, Cassiani G, De Carli M, Bernardi A. An updated ground thermal properties database for GSHP applications. *Geothermics*. 2020;85. http://dx.doi.org/10.1016/j.geothermics.2019.101758.
50. Kaye GWC, Laby TH. *Tables of Physical and Chemical Constants and Some Mathematical Functions*. Fifteenth ed. Harlow, UK: Longman; 1986.
51. McIlveen R. *Fundamentals of Weather and Climate*. New York: Psychology Press; 1998.

52. Busby J, Kingdon A, Williams J. The measured shallow temperature field in Britain. *Q J Eng Geol Hydrogeol*. 2011;44:373–387. http://dx.doi.org/10.1144/1470-9236/10-049.
53. Di Donna A, Laloui L. Numerical analysis of the geotechnical behaviour of energy piles. *Int J Numer Anal Methods Geomech*. 2015;39:861–888. http://dx.doi.org/10.1002/nag.2341.
54. You S, Cheng X, Guo H, Yao Z. In-situ experimental study of heat exchange capacity of CFG pile geothermal exchangers. *Energy Build*. 2014;79:23–31. http://dx.doi.org/10.1016/j.enbuild.2014.04.021.
55. Gao J, Zhang X, Liu J, Li K, Yang J. Numerical and experimental assessment of thermal performance of vertical energy piles: An application. *Appl Energy*. 2008;85:901–910. http://dx.doi.org/10.1016/j.apenergy.2008.02.010.
56. Buhmann P, Moormann C, Westrich B, Pralle N, Friedemann W. Tunnel geothermics—A german experience with renewable energy concepts in tunnel projects. *Geomech Energy Environ*. 2016;8:1–7. http://dx.doi.org/10.1016/j.gete.2016.10.006.
57. Esposito A. *Fluid Power with Applications*. Englewood Cliffs, NJ: Prentice-Hall; 1980.